Solar Energy Materials & Solar Cells 287 (2025) 113593

Contents lists available at ScienceDirect

Solar Energy Materials and Solar Cells

journal homepage: www.elsevier.com/locate/solmat

Transition from silver-to copper-based screen printed SHJ solar cells

S. Pingel [a,*], F.M. Maarouf [a], N. Wengenmeyr [a], M. Linse [a], L. Folcarelli [a], J. Schube [a], S. Hoffmann [a], S. Tepner [b], J. Huyeng [a], A. Lorenz [a], F. Clement [a]

[a] Fraunhofer Institute for Solar Energy Systems ISE, Heidenhofstr. 2, 79110, Freiburg, Germany
[b] Now with EKRA Automatisierungssysteme GmbH, Zeppelinstraße 16, 74357, Bönnigheim, Germany

ARTICLE INFO

Keywords:
Metallization
Heterojunction
Low-temperature paste
Screen printing

ABSTRACT

In this work, we demonstrate the possibility to reduce silver consumption for highly efficient silicon heterojunction (SHJ) cells by screen printing using low temperature paste based on silver, silver-coated copper or pure copper particles. The achieved grid fingers were characterized towards the line and contact resistance as well as the printed width. The most promising pastes with silver or silver-coated-copper particles allow printing of 35 μm narrow fingers with low line resistance of well below 10 Ω/cm. Simulations show that the achieved grid fingers, lead to very low silver consumption. Comparing cost to efficiency optimization shows that the most cost-effective cell has substantially lower efficiency. This might enable the introduction of alternative low silver or silver-free metallization techniques. To show the currently available options to save silver in screen printed busbarless SHJ cells, samples were produced with specific silver consumption of 7.5 mg/W and even below 5 mg/W if the rear side was realized with a pure copper paste. In another test, silver-based cells with same level of efficiency, improved bifaciality and reduced silver laydown (1/3 compared to reference) around 8 mg/W were successfully introduced into modules.

1. Introduction

With further up-scaling of photovoltaics (PV) production worldwide, the reduction of scarce material consumption in solar cell production is gaining major attention. Recent studies have shown that to get silicon heterojunction (SHJ) solar cells to sustainable multi-terawatt production scale, the use of scarce materials like Silver (Ag), Indium (In) and Bismuth (Bi) must be drastically reduced [1–5]. According to Zhang et al. [3], the specific consumption of Ag for solar cells must be limited to only 2 mg/W in the long-term to be compatible with global resources, down from 15.5 mg/W in 2023 for SHJ cells according to Chang et al. [5].

For SHJ metallization low-temperature pastes (LTP) are typically cured at temperatures of around 200 °C for a few minutes [6]. Compared to PERC or TOPCon, where high temperature firing is used, the sintering of the Ag particles is less efficient in LTP. There are different approaches for screen printing to reduce the Ag consumption in solar cells, the most relevant are.

- Application of fine-line grid fingers by screen printing process, paste and screen optimization [7].
- Reduction of the Ag content in the paste, by replacing Ag as conductive particles with Ag-coated copper (Cu) particles (AgCu) [8].
- Complete replacement of Ag pastes with Cu pastes [9–12].

The industrial standard process for metallization with low or high temperature pastes is flatbed screen printing (FSP) [13]. This technology is expected to remain the dominant process for Si solar cell metallization due to its cost-effectiveness and flexibility towards a fast-evolving PV market [14,15]. Other Ag-LTP or Ag-ink metallization technologies are in the developing phase or shortly before industrialization, for example Rotary Screen Printing [16], FlexTrail [17] or Dispensing [18–20]. AgCu- or pure Cu-LTP can be applied by the techniques mentioned above whilst a number of institutes and companies are also working on Cu-plating: Sundrive, PV2+, Sunwell [21–27]. The use of Cu in metallization bears risks for i) cell performance degradation (due to Si base contamination) and ii) the manufacturability or module reliability (due to oxidation on the metal surface). However, first testing shows good

This article is part of a special issue entitled: MIW2024 proceedings published in Solar Energy Materials and Solar Cells.

* Corresponding author.
E-mail address: sebastian.pingel@ise.fraunhofer.de (S. Pingel).

https://doi.org/10.1016/j.solmat.2025.113593
Received 30 January 2025; Received in revised form 12 March 2025; Accepted 17 March 2025
Available online 9 April 2025

results for TOPCon and SHJ [9,11,12,28]. In this work, we focus on the currently industrially established metallization technique for SHJ cells: screen printing of LTP based on Ag or AgCu particles, but also present some first results of cells metallized with Cu paste.

2. Material and methods

This paper consists out of four parts, summarized in Table 1. In the first part (1) a data set from paste screening is generated by printing of dedicated test patterns with varying line widths on SHJ precursors. Different Ag and AgCu pastes are used and subsequently the grid resistance and contact resistance is measured and combined with microscopy analysis of the finger geometry. In part (2) grid simulations are then used to investigate suitability of the printed fingers for module integration with respect to highest efficiency η or lowest costs.

In part (3) pastes ranking among the best in the prior screening were selected and cells were produced with varied front and rear side (FS and RS) combinations of Ag and AgCu pastes. Here, also Cu paste was applied on the RS to show the potential of completely Ag-free pastes when finger shading is less relevant.

In part (4) different layouts printed with Ag paste were combined on FS and RS of industrial precursors. After separation the half-cut cells were integrated into modules and characterized.

2.1. LTP screening with test forms

To investigate the fine-line capability of different pastes at Fraunhofer ISE specific test forms have been designed [29], see Fig. 1. These allow the evaluation of various screen openings/nominal finger widths w_N on a single wafer, relying on high-throughput analysis using industrial cell characterization. With this approach the compatibility of the pastes with various w_N can be investigated on the same wafer.

These screens were used on the RS of industrial SHJ-precursors (M6/166 mm wafer format) after transparent conductive oxide (TCO) deposition. The test forms consist of 0BB-layouts and five busbars (5BB) were applied in a second (dual) printing step using an ASYS EKRA screen printing line at Fraunhofer ISE PVTEC. On the FS of the cells a reference 5BB metallization layout was applied beforehand. After each print step, the laydown M was recorded and a short drying cycle at 200 °C for 1 min was applied. After the last printing step, the dryer temperature was increased to 220 °C, acting as a quick 1 min curing step.

After metallization, the samples were finished and prepared for *I-V* evaluation at a HALM cell tester. Additionally, the four grid resistances $R_{grid}\ (w_{N,i})$ (i = 1 to 4) between the 5 busbars were measured. The average line resistance values R_{LINE} for each segment were calculated by the following equation (1):

$$R_{LINE}(w_{N,i}) = R_{grid}(w_{N,i})\,\frac{n_F}{d_{BB}} \tag{1}$$

Table 1
Overview of the experimental and simulation steps presented in this paper.

Part	Section	Type	Sample	Target
1	2.1/3.1	Exp.	M6 (166 mm) FC 5BB	Data generation with test forms for Ag and AgCu pastes: $w_F/R_{LINE}/\rho_C$ (paste, w_N, …)
2	2.2/3.2	Sim.	M10 (182 mm) HC 20 wires	GridMaster simulation with varied finger pitch for 20 wires. Optimization on high η or low costs.
3	2.3/3.3	Exp.	M6 (166 mm) FC 0BB	Production of 0BB solar cells with different combinations of Ag, AgCu and Cu pastes. η vs. Ag consumption.
4	2.4/3.4	Exp.	M6 (166 mm) HC 16 wires	Production of 0BB solar cells with varied layouts on FS and RS with one Ag LTP. Module integration of half cut cells.

Using the number of printed fingers n_F between the busbars (here 127, leading to a finger pitch of 1.3 mm for M6 wafers) and the distance between the busbars d_{BB} is considered to calculate the average R_{LINE}.

To further evaluate the printed fingers in the different segments confocal laser scanning microscopy (CLSM) images were captured with an Olympus LEXT microscope and analyzed by the software tool DASH, developed at Fraunhofer ISE [30]. Besides the printed (or shading) finger width w_F, further geometrical data such as finger cross-section area A_F and core finger width w_C was extracted. The silver laydown per finger $m_{Ag,F}$ for the nominal opening $w_{N,i}$, where i is again the parameter between 1 and 4 (different segments in Fig. 1), was estimated by the weighting equation (2).

$$m_{Ag,F}(w_{N,i}) = \frac{M}{n_F} \times \frac{5 \times A_F(w_{N,i})}{1.5 \times A_F(w_{N,1}) + A_F(w_{N,2}) + A_F(w_{N,3}) + 1.5 \times A_F(w_{N,4})} \times f_{Ag} \tag{2}$$

The first factor is the average laydown per finger that is calculated by dividing the wet laydown M by the total number of fingers n_F. The second factor is weighting the laydown by the finger cross section areas A_F for the different $w_{N,i}$. Here it is assumed that the A_F scales linear with $m_{Ag,F}$. The segments 1 and 4 are weighted by a factor of 1.5 since the top and bottom part outside the area used for grid resistance measurements have the same w_N as the neighboring segments. Finally, the parameter f_{Ag} is the mass fraction of silver in the paste that ranges typically around 92 %$_{wt}$ for Ag LTP and between 35 and 65 %$_{wt}$ for AgCu in this study, correspondingly f_{Cu} is the mass fraction of copper. In this experiment, thirteen Ag and seven AgCu pastes with different values for f_{Ag} were tested and evaluated, as shown in Fig. 2. Eleven Ag pastes were printed with a fine-line screen that has suitable w_N especially for the FS application while the seven AgCu pastes and two RS Ag references were printed with an angled screen with larger w_N, smaller mesh count and wider wires.

To illustrate the advancements in terms of Ag reduction, the effective silver usage parameter λ_{ESU} [19] is calculated according to equation (3) where the finger length on the wafer l_F is considered compared to the achieved R_{LINE} and the used silver amount per finger:

$$\lambda_{ESU}(w_N) = \frac{l_F}{R_{LINE}(w_N) \times m_{Ag,F}(w_N)} \tag{3}$$

Besides the parameters dealing with the lateral finger resistance and Ag consumption also the vertical resistance between TCO and metal is a relevant parameter for the device performance. For its determination stripes with constant w_N were extracted by laser separation and sheet resistance R_{sh} and contact resistivity ρ_c was determined with the TLM method using a TLM-Scan setup from PV-Tools. For the contact finger width in the TLM model, the measured core finger width w_C was used, since the parameter is more robust compared to w_F and part of the bleed-out area might not be well contacted. This leads to a potential underestimation of the actual ρ_c since the real width of the contacted area lies between w_F and w_C.

2.2. Simulation with GridMaster

The parameters w_F (grid shading), R_{LINE} (series resistance losses within grid) and contact resistivity ρ_c from the paste screening were used to optimize the metallization layout by simulation, targeting high cell η for each paste and w_N. To evaluate the impact of these three parameters for a fixed interconnection, the tool GridMaster, developed at Fraunhofer ISE, was used for performance simulation [31].

The expected η was simulated for a bifacial scenario with 1000 W/m^2 FS and 100 W/m^2 RS illumination. For the cells the number of fingers/finger pitch on the FS or RS ($n_{F,FS}$, $n_{F,RS}/p_{F,FS}$, $p_{F,RS}$) was varied while the shading and resistance of the interconnection wires was neglected since their impact is comparable for the simulated scenarios. The finger

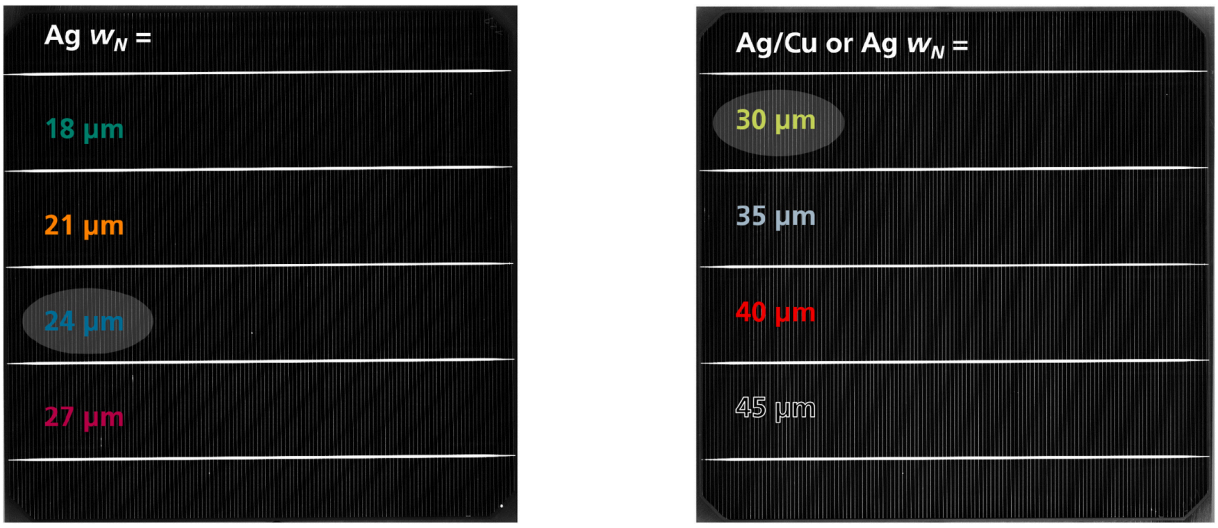

Fig. 1. Test form layout with varied nominal finger width for Ag paste and AgCu/RS Ag pastes. The data from the two highlighted nominal finger width are presented in the paper.

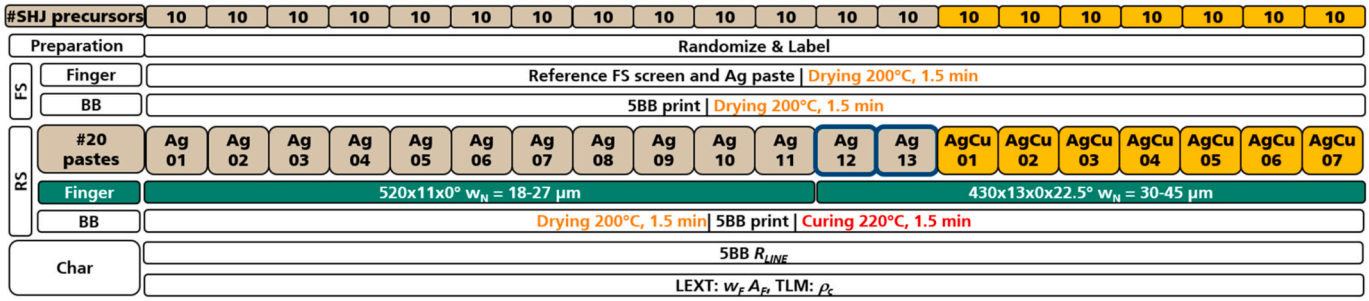

Fig. 2. Paste screening process flow.

shading width was assumed to match the printed finger width w_F.

Further parameters used for the simulation are summarized in Table 2 below. Photon generation and dark saturation current parameters were adapted to simulate SHJ precursors with a potential of η = 25.5 % without metallization related losses (no shading, no R_{LINE} and ρ_c losses).

For each paste the $p_{F,FS}$ and $p_{F,RS}$ was optimized for highest η with the boundary condition $p_{F,RS} \geq 0.87$ mm. Since RS paste consumption is only marginally affecting the shading for low RS irradiations the highest η was found for all pastes for the smallest $p_{F,RS}$.

Besides η-optimization also a cost optimization was conducted. As a reference, the m_{Ag} value given in Ref. [5] was used (13.9 mg/W on cell level, assumed an Ag LTP with 92 % Ag content, 24.5 % assumed η).

Table 2
Overview of the parameters used in the GridMaster simulation.

Description	Parameter	Value
Cell edge length	L	182 mm (M10)
Module wires	n_{BB}	20 wires (⌀ 250 µm), 9.1 mm wire pitch, resistance and shading neglected
TCO sheet resistance FS and RS	R_{SH}	140 Ω/
Silicon bulk resistivity	$\rho_{Si,bulk}$	1 Ωcm
Wafer thickness	d_W	110 µm
FS/RS irradiation	$Irr_{FS,RS}$	1.0/0.1 sun equivalent
Shading width	w_F	Data from 3.1
Line Resistance	R_{LINE}	
Contact resistivity	$\rho_{metal,TCO}$	
FS # fingers, pitch	$n_{F,FS}$, $p_{F,FS}$	Varied
RS # fingers, pitch	$n_{F,RS}$, $p_{F,RS}$	Varied

Compared to this reference the change in η and cost for metallization were considered.

The paste price P_{paste} was calculated by a simple model according to equation (4) that roughly fits to the relative price difference given by the company Fusion in Taiyang News Presentation [32] for different Ag Cu blending ratios. The parameters their values are summarized in Table 3.

$$P_{paste} = PCF_{prod} \times \left(f_{Ag} \times P_{Ag} + f_{Cu} \times P_{Cu}\right) \quad (4)$$

For each paste and pitch the paste consumption was calculated as well as the costs due to the paste consumption.

The added value or added price AP compared to the reference was then calculated by equation (5). Potential differences in screen costs were neglected because no data for the reference was available.

$$AP = \frac{\left(P_{mpp} - P_{mpp,Ref}\right) \times P_{cell} - \left(M \times P_{paste} - M_{Ref} \times P_{paste,Ref}\right)}{P_{mpp}} \quad (5)$$

P_{mpp} corresponds to the cell power under Standard Testing Conditions (STC: 1000W/m^2, 25 °C) and P_{cell} to the price of the cell, M to the paste laydown and P_{paste} to the price of the paste.

Table 3
Cost model parameters for Ag and AgCu pastes.

Description	Parameter	Value
Cell price	P_{cell}	0.1 €/W
Ag price	P_{Ag}	1000 €/kg
Cu price	P_{Cu}	458 €/kg
Paste production cost factor	PCF_{prod}	1.3

The index *Ref* refers to the (partially) assumed parameters of the reference cell [5]. Here a 9BB cell is mentioned and with a m_{Ag} of 17.1 mg/W on module level where BB and tab contribute about 4.2 mg/W. This leads to a m_{Ag} of 13.9 mg/W for a not optimized busbarless cell. For the best performing paste and w_N combinations for both Ag and AgCu paste, the highest *AP* simulation was selected and compared to the η-optimized simulation.

2.3. Cell production

To test the compatibility of well performing pastes with potentially low Ag consumption from the paste screening, cells were produced on basis of industrial SHJ solar cell M6 precursors. The process flow with different combinations of Ag 03 and AgCu 04 is shown in Fig. 3a).

The wet paste laydown *M* was measured after each print step in this experiment, except for all print steps with Ag 03, where existing data from previous experiments had to be used, due to malfunction of the scale. After the final curing the cells were measured in 5BB and 9BB configuration on a conductive chuck with black cuck J_{SC} calibration. For comparability with industrial 0BB SHJ cells 18 wire module-configuration (18BB) were extrapolated according to Ref. [33], based on the 9BB IV measurement using the R_{LINE} from 5BB. In an additional batch the compatibility of the pastes Cu 01 was compared to the Ag 01 paste for application on the RS, see Fig. 3b). Here two cases were compared: i) wide fingers ($w_N = 80$ µm) and ii) narrow fingers ($w_N = 25$ µm) on the RS. The FS was metallized with a reference layout and paste Ag 01. The curing conditions in this batch varies. The expected impact of the different curing profiles on the metallization is rather small, since the Ag 01 pastes is an ultra-low temperature paste curable at even lower temperatures than 180 °C.

2.4. Module integration

In a third batch, cells were produced on M6 industrial SHJ precursors. Here, the metallization layout was varied on FS and RS of the cells. Different screens were combined on FS and RS with varying w_N (14–30 µm), p_F (0.6–2.1 mm) and mesh type, see Fig. 4. For all layouts pastes Ag 01 was used and after all print steps the wet laydown *M* was recorded. The RS was printed first, followed by a drying step at 200 °C for 1 min. Then FS was printed with a subsequent short curing step at 220 °C for 1 min. The cells were then separated to half cut by a Laser Scribe Mechanical Cleave (LSMC) process and after *I-V* stringed to half-cut cell strings by a wire soldering process suitable for busbarless cells.

Per combination 2–3 half-cut cell strings were then integrated into bifacial glass-glass modules (3 mm float glass, POE encapsulation) and the characterized with an *I-V* tester. Both the full area and masked area (70 % open area) *I-V*-curve and electroluminescence (EL) images were recorded. The masked *I-V* was necessary for a fair comparison since the module wires did not contact the grid fingers in the perimeter area of the solar cells for all samples. The cells were measured on FS and RS to enable the determination of the bifaciality or back to front ratio *BFR*.

3. Results and discussion

In this section the results of paste screening, the simulation as well as the two cell batches and one module batch is reported. In the last part the experimental results are compared in terms of specific silver consumption with values from literature and put into the context of upcoming developments.

3.1. LTP screening with test forms

Different finger widths were tested according to Figs. 1 and 2. For further analysis, we focused on the data of $w_N = 24$ µm for Ag pastes and $w_N = 30$ µm for AgCu pastes, which gave reasonable printing results for all tested pastes and allow a fair comparison in the achieved printed width w_F. Notably, for Ag pastes also for smaller w_N suitable results were achieved. From the *I-V* measurements of the paste screening samples the R_{LINE} was extracted by equation (1), the results are presented Fig. 5a). Based on equation (3) from the A_F weighted laydown $m_{Ag,F}$ the λ_{ESU} was determined, shown in Fig. 5b). As third parameter the w_F is presented in Fig. 6a). For these three parameters the data is shown only for $w_N = 24$ and 30 µm in Fig. 5a)-b) and 6. a) due to better clarity and comparability in the w_F for both Ag and AgCu pastes. As last parameter the ρ_c shown in Fig. 6b) not separated for the different w_N.

Most Ag pastes could be printed with $w_N \geq 21$ µm and gave suitable low R_{LINE} values. For $w_N = 18$ µm only two pastes (Ag 07 and Ag 10) achieved $R_{LINE} < 5$ Ω/cm. For $w_N \geq 24$ µm all pastes besides Ag 04 show similar level of R_{LINE} in the range 2–4 Ω/cm. For AgCu the variability in R_{LINE} for $w_N = 30$ µm is larger. Only AgCu 04 and AgCu 05 are on a similar level as the RS Ag 13 reference slightly above $R_{LINE} = 2$ Ω/cm. This is due to the differences in compatibility with the 430 × 13 × 22.5° mesh. With increasing w_N the variability in R_{LINE} reduced substantially but the data is not presented here.

For the Ag pastes with a typical Ag content around 92 % the λ_{ESU} varies in a band between 15 and 25 cm^2/(Ω mg) for $w_N = 24$ µm, besides the outlier Ag 04. Most of the AgCu pastes did not clearly outperform the Ag RS reference pastes (Ag 12 and Ag 13) printed with the same w_N. This is a surprise since the Cu content in AgCu varied roughly between 25 and 60 %$_{wt}$ (leading to a reduced Ag between 35 and 65 %$_{wt}$). For most AgCu pastes printing issues or incompatibility with the mesh-opening (w_N = 30 µm) combination led to only marginally improved λ_{ESU}. Only AgCu 04 and AgCu 05 achieved low R_{LINE} and had a low Ag in parallel, leading to superior λ_{ESU} level above 50 cm^2/(Ω mg). Compared to the best λ_{ESU} of the Ag pastes for $w_N = 24$ µm, this leads to factor >2 improved λ_{ESU} for these two AgCu pastes.

Coming to the third investigated parameter w_F reveals significant differences between the pastes. The median printed w_F for both pastes types and w_N shows a minimum at $w_{F,min}$ ~35 µm and a maximum at $w_{F,max}$ ~52 µm, leading to a range of ~17 µm. Using narrow fingers as

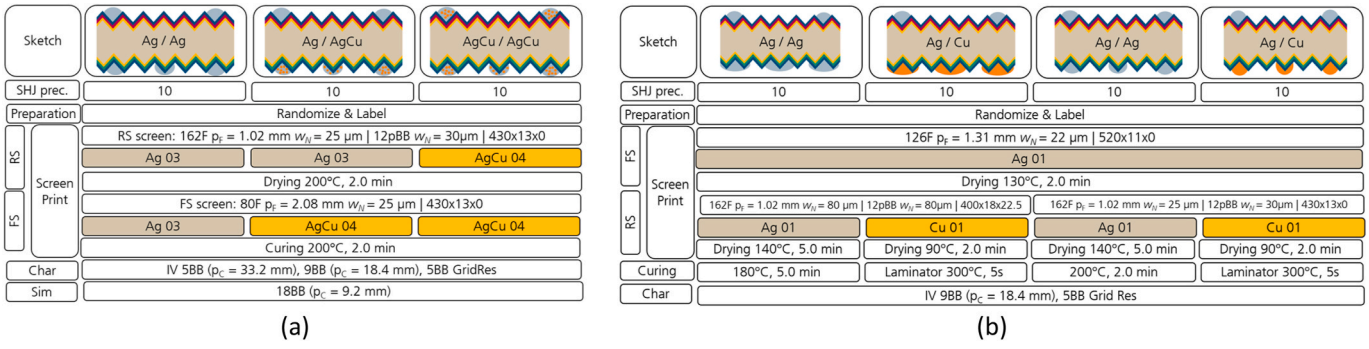

Fig. 3. Process flow of cell batch 1 a.) Ag vs. AgCu and cell batch 2 b) Ag vs. Cu on the RS.

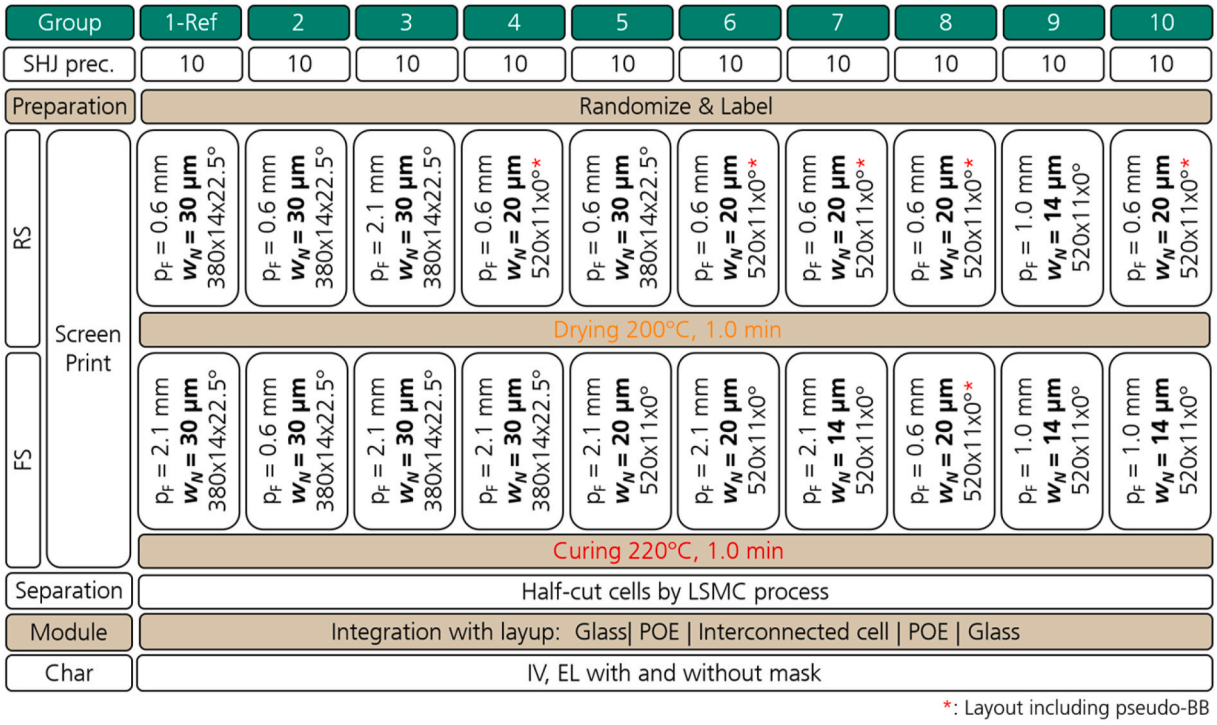

Fig. 4. Cell batch 3 for module integration with varied layouts on FS and RS.

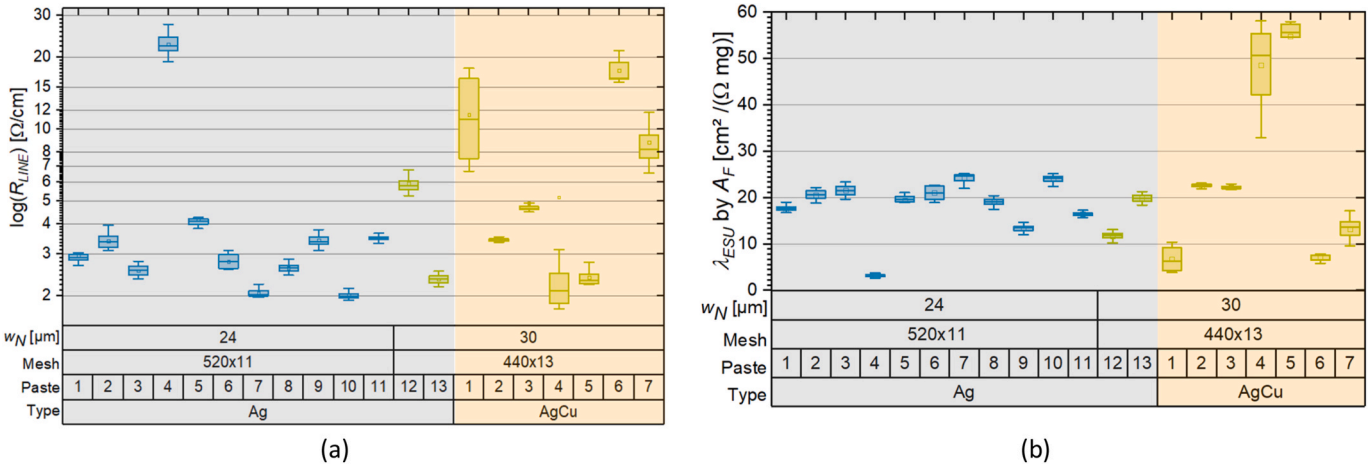

Fig. 5. Data from Ag and AgCu paste screening for w_N = 24 and 30 µm, (a) Line resistance R_{LINE}, (b) Effective Silver usage λ_{ESU}.

reference and comparing to the widest printed fingers means about 50 % increased shading. This will have a strong impact on the optimal number of fingers since the shading is the most important parameter when losses due to metallization are investigated.

The last shown parameter is ρ_c. Here, differences are rather small for the Ag pastes: all had $\rho_c < 0.4$ mΩcm^2 leading to a rather small impact of ρ_c on the performance of the cell. For AgCu the results are different, only the pastes AgCu 06–07 show a low ρ_c comparable to pure Ag paste, while AgCu 01–03 vary in the range 0.5–0.6 mΩcm^2 and AgCu 04–05 had even higher ρ_c between 0.8 and 1.0 mΩcm^2. An important factor might be the AgCu particle size and shape. Ag04-05 achieved the best R_{LINE} but show rather high ρ_c, potentially larger particles are beneficial for low Ag consumption and low R_{LINE} but low resistance contacting of the textured sample surface might here be more challenging.

3.2. Simulation with GridMaster

Simulation on basis of the data from the paste screening showed that AgCu pastes perform lower in η and added price AP due to lower screen but also lower paste quality. The results of the simulation are shown in Fig. 7, in the left part the simulated η is plotted versus the m_{Ag} and on the right part the added price AP versus the m_{Ag}. In both graphs the simulation results for Ag (blue) and AgCu (orange) pastes are shown for the two scenarios of cost- and η-optimization (closed and open symbols). An interesting aspect is that m_{Ag} is not substantially improved for the AgCu pastes since paste consumption is higher compared to the finer printed Ag lines but also the λ_{ESU} was not improved substantially for small w_N for most AgCu pastes and if it was improved (AgCu 04 and 05) it came along with high ρ_c leading to an η-penalty. In the follow up experiment all pastes will be printed with the same fine-line mesh and w_N to have a fairer comparison.

The simulation boundary conditions, low cell price (0.1 €/W$_p$) and

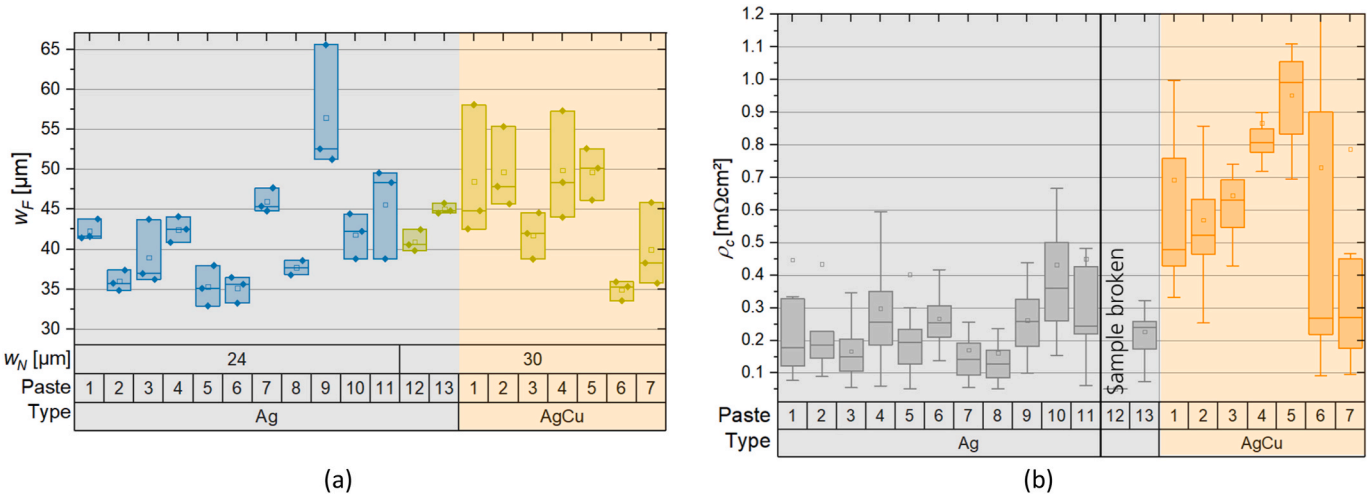

Fig. 6. Data from Ag and AgCu paste screening. (a) printed width w_F for w_N = 24 and 30 µm, (b) contact resistivity ρ_c for all w_N.

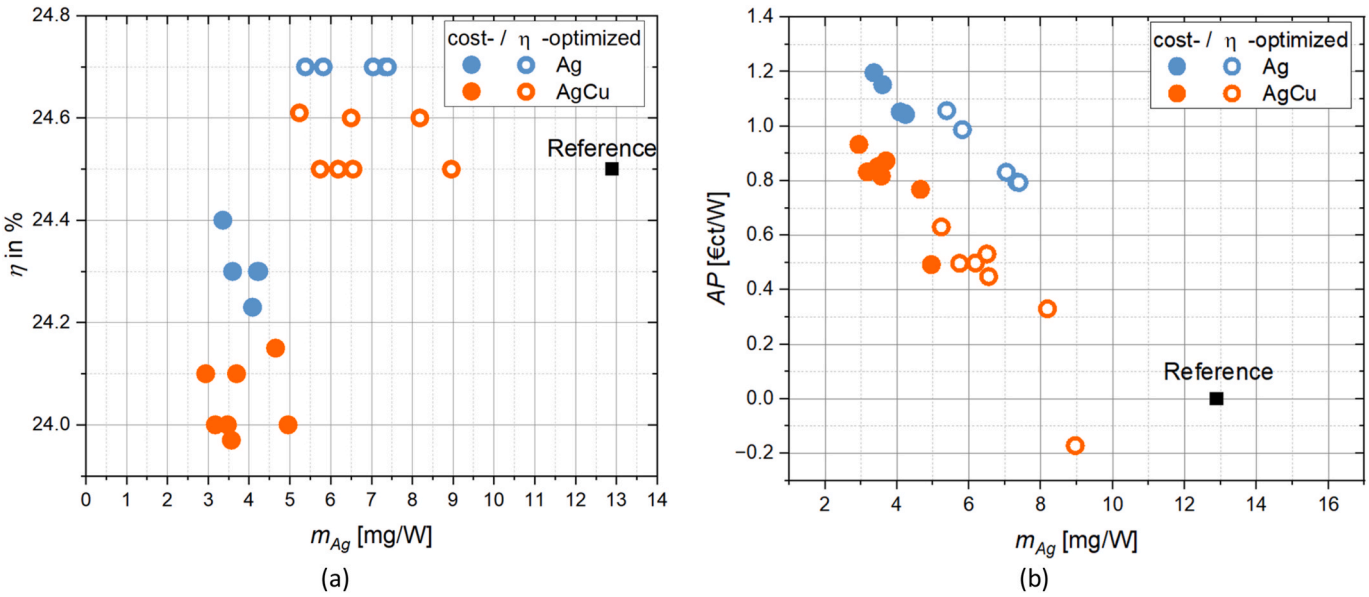

Fig. 7. Simulated η (a) and added price AP (b) for cells based on Ag and AgCu pastes investigated for the two scenarios: η- and cost-optimization.

high Ag price (1000 €/kg), have a strong impact on the cost-optimization scenario. The more expansive the Ag and less valuable the cell power the larger difference between the η- and cost-optimized scenario. For the chosen parameters in this investigation, we found ~0.4 $\%_{abs}$ lower η and ~3 mg/W lower m_{Ag} for the cost optimized scenario, both valid for Ag and AgCu.

Compared to the reference (m_{Ag} = 12.9 mg/W, assumed η = 24.5 % [5]) the investigated pastes lead to a similar or slightly higher simulated η-level, but this is achieved for a substantially lower m_{Ag} already in the η-optimized scenario. If costs due to paste consumption are considered the resulting η is lower than the reference but for this rather aggressive scenario the AP is the highest and m_{Ag} lies in the range 3–5 mg/W. This substantial difference in η due to the price of the consumables leads to a window of opportunity for alternative low-Ag or Ag-free metallization technologies. The silver price will likely increase in the future, but the development of the cell price is hard to predict in the current consolidation phase of the PV industry.

3.3. Demonstration of AgCu paste on full cells

SHJ solar cells with Ag/Ag, Ag/AgCu and AgCu/AgCu configuration were produced according to the proces shown in Fig. 3a), for this the pastes Ag 03 and AgCu 04 were used. The *I-V* results are shown in Fig. 8. The short circuit current density J_{SC} is ~0.2 mA/cm^2 higher for Ag 03, indicating finer lines, for the same applied screen. The wider AgCu fingers and larger cross-section A_F lead to more shading which is over-compensated by *FF* improvement when AgCu is printed on the FS, resulting in improved η. This is visible clearly for the 5BB *I-V* but also for 9BB the *FF* increases for AgCu 04 on the FS.

For the η only 5BB profits clearly from the lower R_{LINE}. For 9BB all groups are on a similar level. For the simulated 18 BB η the group combining fine-line printable Ag on the FS and AgCu on the RS performs best. This confirms the findings in Ref. [7] where we found that fine-line LTP metallization is especially compatible with small wire pitches.

For AgCu 04, a laydown of about 32 mg on the FS and 72 mg on RS was recorded. The RS laydown is higher per finger due to the additional pseudo-busbar (pBB) in the layout that leads to about 10 % higher laydown. In total this sums up to 104 mg AgCu paste. With an Ag content

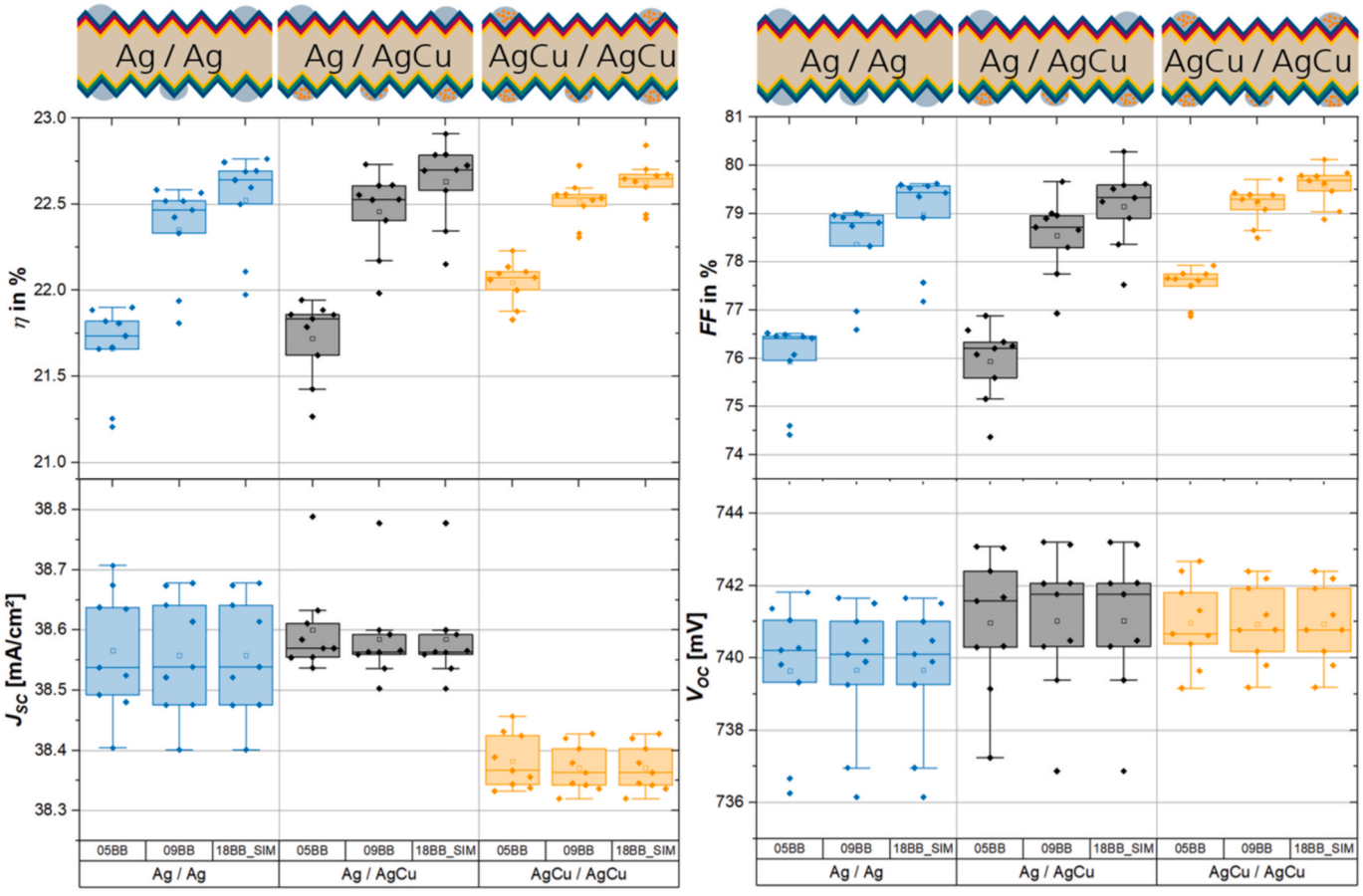

Fig. 8. Measured (5BB and 9BB) and simulated (18BB) *I-V* data for cell batch 1 with Ag and AgCu pastes.

of 45 % the cells of the last group AgCu/AgCu were produced with about 47 mg Ag. The corresponding m_{Ag} for the 9BB measurement (6.14 W) is 7.7 mg/W and slightly lower for the simulated 18BB resulting in ~7.5 mg/W. Correcting for the estimated laydown of the pBB results in about 7 mg/W.

The laydown of Ag 03 could not be recorded in this experiment. The wet laydown *M* for Ag 03 is expected to be significantly lower since R_{LINE} was substantially higher compared to AgCu 4. The specific m_{Ag} is roughly estimated to be $m_{Ag} < 10$ mg/W based on earlier experiments with the same paste.

In the second cell batch, the compatibility with Cu paste applied on the SHJ cell RS side was investigated. The cells were produced all with the same Ag 01 LTP and layout on the FS while the RS was varied with two w_N and two pastes (Ag 01 and the copper paste Cu 01) on the RS

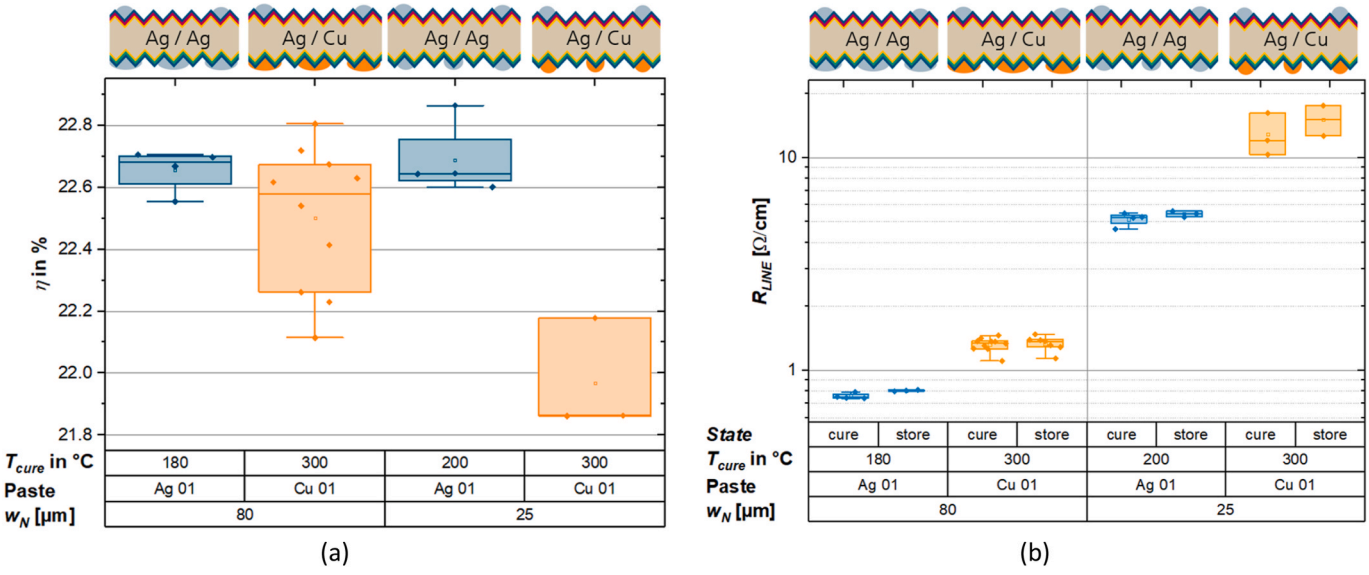

Fig. 9. (a) Measured η-data with 9BB contacting for cell batch 2 with Ag and Cu paste and (b) 5BB R_{LINE} measurement after curing and 24 days storage in air.

according to the process flow in Fig. 3b).

Comparing the two groups in Fig. 9a.) printed with the large w_N on the RS reveals a small drop for the median η of about 0.1 % when the Cu paste is compared to the Ag paste. The reproducibility for the Cu group is worse, due to several reasons (offline manual printing of Cu paste, handling issues, different curing processes compared to automated printing process for the Ag paste).

For a narrow w_N of 25 µm, the Ag group stayed on a similar level as for 80 µm while the Cu group lost about 0.6 $\%_{abs}$ in η compared to Ag. The reduction in *FF* is indicating series resistance R_S issues. The loss is not caused by the larger R_{LINE} for Cu groups that is shown in Fig. 9.b), because the cells were measured FS up with the varied RS on a conductive chuck, but the root cause for the η-loss is more likely due to issues with ρ_c on the RS. In TLM measurements Ag01 showed ρ_c ~0.2 $m\Omega cm^2$ (compare to Fig. 6b) and the Cu paste had a ρ_c ~5 $m\Omega cm^2$ for w_N = 80 µm. The more than one magnitude larger ρ_c for Cu plays a more pronounced role for the narrow fingers since the contacted areas are reduced by about factor larger than 2. The Cu paste seems not yet ready for fine-line contacts due to the high ρ_c.

The cells were also measured RS up in 5BB configuration to determine the R_{LINE}. The samples were measured after curing and after 24 days of storage in air. The data is shown in Fig. 9b). The R_{LINE} did not chance significantly indicting that the bulk and surface of the pastes is not significantly oxidizing. This is already a good indication for the stability of the paste in a production environment but needs to be followed up by reliability tests on module level.

3.4. Module integration

In the third batch SHJ cells with varied metallization layouts, summarized in Fig. 4, were produced. After module integration the two half-cut cell modules were characterized with EL. Images of full area and masked module are shown in Fig. 10. In the lower edges of the full area EL image contact issues are visible as dark areas. Here the interconnection wire does not contact the grid fingers close to the cell edge. The metallization was not adapted in all cases for module integration leading to a high R_S in this cell perimeter area for many modules. Depending on the cell metallization the gain from full area to masked IV was 0.2–1.3 $\%_{abs}$ in η. The larger p_F and the finer the fingers the more pronounced the found η-gain.

To have a fairer comparison the modules were all measured with the mask. The found power measured under STC was corrected for the masked area and was put into perspective of the Ag content of the cell laydown *M*. The median values of masked η-data versus the specific m_{Ag} are plotted in Fig. 11.

The group with the lowest m_{Ag} was printed with $w_N = 14$ µm layouts (group 9) and it was compared to the group printed with reference layouts (group 1). The specific Ag laydown could be reduced from 21.1 mg/W to 7.9 mg/W, cutting the Ag consumption almost by two third as shown in Table 4 below. The *I-V* parameters changed only slightly besides the series resistance R_S that is clearly increasing for the low Ag samples. The reference had a lower open circuit voltage V_{OC} that can not only be explained by the differences in metallization and is more likely caused by differences in precursors quality (even though randomization of the precursors) and/or handling defects introduced during cell and module fabrication. The short circuit current density J_{SC} of the low Ag group is even smaller compared to the reference but the FF is higher due to the finer pitch and again likely due to precursor quality. Taken all together this leads to a 1 $\%_{rel}$ improved η. Besides the laydown reduction clearly improved is also the bifaciality/*BFR* due to less metal coverage on the RS because of fine-line printing and adapted p_F for the low Ag group. Overall, the low Ag metallization worked well, and it was shown that the IV parameters are in sum not negative affected by the reduced

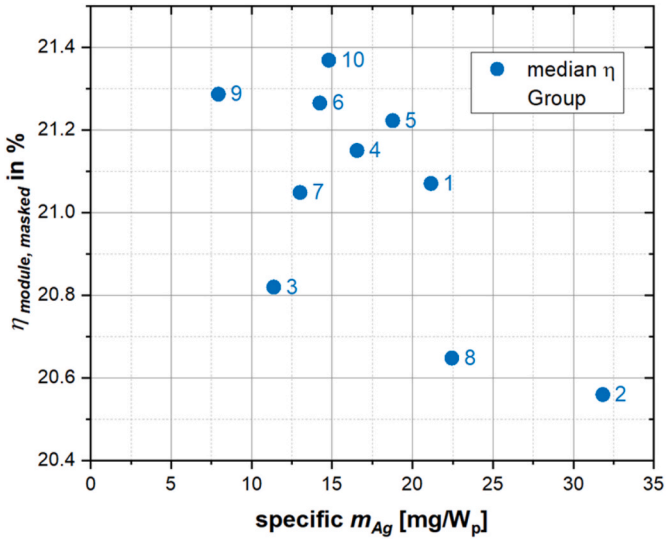

Fig. 11. Masked module η-data over specific Ag consumption m_{Ag} for the different cells with different combinations of FS and RS metallization layouts, the labeling represents the group ID from Fig. 4.

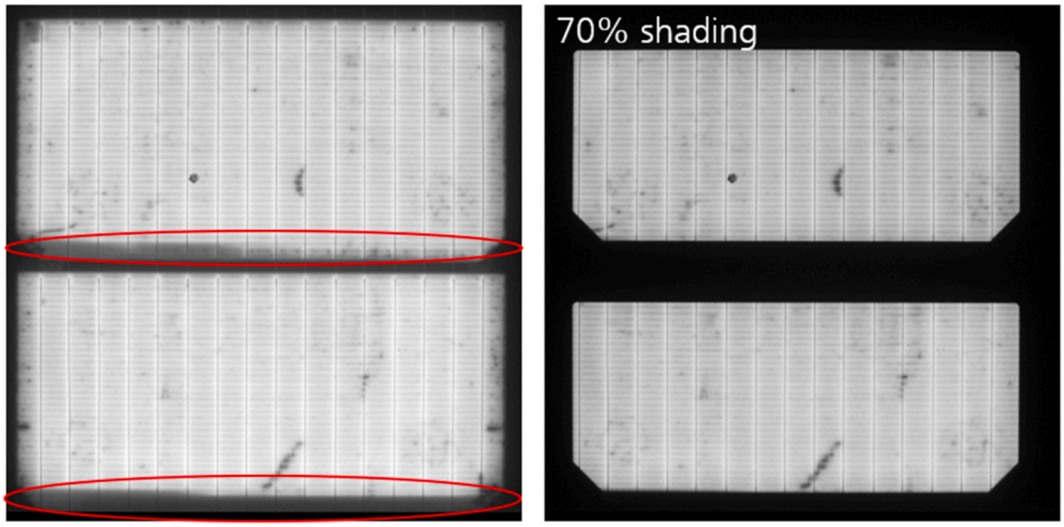

Fig. 10. EL images of a module without (left) and with mask (right). Showing the non-uniform wire contact due to not adapted metallization.

Table 4
Median module data of the reference and lowest m_{Ag} group.

Parameter	$p_{F,FS}/p_{F,R}$	m_{Ag}	V_{OC}[a]	J_{SC}	FF	η	R_S[a]	BFR
Units	[mm]	[mg/W]	[mV]	[mA/cm^2]	in %	in %	[mOhmcm^2]	in %
Group 1-Ref	2.1/0.6	21.1	729	35.9	80.5	21.1	0.9	94.7
Group 9	1.0/1.0	7.9	735	35.7	81.0	21.3	1.1	95.6
Rel. change		**−62.6 %**	0.8 %	−0.4 %	0.6 %	1.0 %	21.6 %	**1.0 %**

[a] per half-cut cell.

Ag consumption. A clearer comparison would require better statistics and not only 2–3 small area modules per variation.

3.5. Classification of the results

The results from the three cell/module batches are shown in Fig. 12 below together with the published data [3,5]. The results of the latest cell batches are well aligned with other achievements in industry, e.g. Risen claimed to have achieved 7 mg/W. Taken all together this indicates a rapid reduction of Ag consumption in SHJ cells and that the mid-term goal of 5 mg/W given in Ref. [5] is within reach and will likely be achieved in the next two years. The long-term goal of 2 mg/W is more challenging and will require a substantial improvement of the AgCu pastes or the application of pure Cu pastes.

4. Conclusions

In this work we present tests results of Ag and AgCu LTPs for SHJ cells. Compared to Ag pastes with >90 %$_{wt}$ Ag the investigated AgCu pastes had an Ag content in the range 35–65 %$_{wt}$. This reduction is expected to lead to an improved Ag utilization λ_{ESU}. For narrow w_N of 30 µm only two AgCu pastes showed a clear improvement by a factor of 2 or greater. For larger w_N, not shown, two more pastes had an increase in λ_{ESU} compared to pure Ag but three pastes did not show any appreciable improvement compared to Ag at all. One reason might be the unequal comparison of 0° screen for Ag pastes and 22.5° screen for AgCu but this alone can't explain the findings. In an upcoming paste screening, we will use the same screens for both type of pastes for a fair comparison. One key finding is that also AgCu pastes need to be fine-line compatible since they still contain a certain amount of Ag and for a large A_F, they can't compete with high performance fine-line Ag fingers. With further decreasing Ag content in AgCu this assessment might change since the paste suppliers already work with paste <30 %$_{wt}$ Ag but especially on the cell FS a fine-line solution is necessary for high η cells, if bifaciality is important fine-line is essential also on the rear. In summary the challenge for the paste suppliers is to provide pastes that offer good printability enabling high throughput and in parallel allow a fine-line print with low Ag consumption, low R_{LINE}, low w_F, low A_F and finally a low ρ_c. The last parameter seems to be a special challenge for AgCu paste with low Ag content and high λ_{ESU} since ρ_c was found to be significantly higher for those pastes, potentially due to larger particles.

The data from the paste screening was fed into GridMaster simulations to optimize the metallization layout of bifacial cells. The optimization was done for two targets: (i) for high η and (ii) low cost. For low-cost optimization the Ag/AgCu consumption at a low cell price was balanced with the decreasing value of the cell due to lower η. The results: Ag pastes performed better in η and cost but at least partially this can be explained by the differences in the quality of the used screens. The best AgCu pastes had a slight advantage in m_{Ag}, but this did not lead to better cost structure. Comparing the two optimization scenarios (i) and (ii) the m_{Ag} improved from about 5.5 to 3.5 mg/W showing that for busbarless cells the mid-term goal of 5 mg/W is clearly within reach for both Ag and AgCu metallization without severe η-penalty. The cost optimized scenario leads to a substantial loss in η of about 0.3–0.4 %$_{abs.}$ compared to

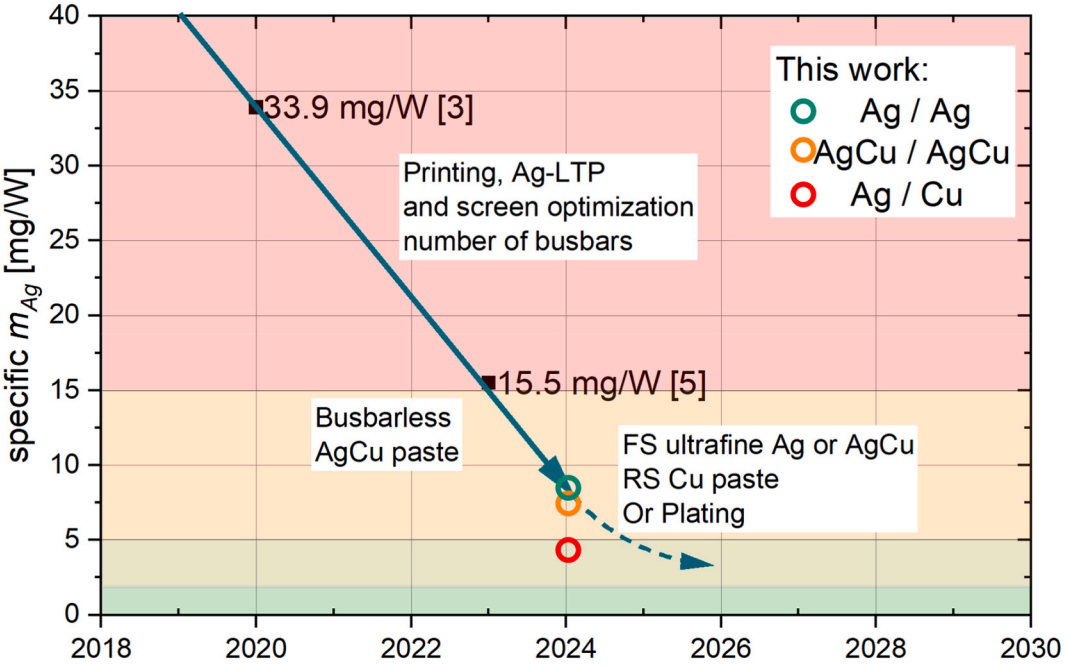

Fig. 12. Rapid development of the reduction of Ag consumption in the last few years for SHJ solar cells. Extrapolation indicates that 5 mg/W will soon be passed likely with optimization of Ag and AgCu pastes (and higher cell η) while 2 mg/W might make the introduction of Cu paste or alternatives necessary.

η-optimization. This huge drop indicates a window of opportunity for further screen-printing optimization or other fine-line low Ag or even Ag-free SHJ metallization techniques. For screen printing it will be necessary to continue the development of screens and pastes to reduce the costs when going fine-line. Due to the high Cu content in AgCu pastes, it is expected that their prices will significantly decrease in the future compared to silver pastes. As these pastes are becoming already mainstream and production scales up, the costs associated with their rapid development will be reduced over time.

In the first cell batch, the fine-line compatibility of AgCu was investigated. If AgCu is applied on FS and RS a m_{Ag} of 7.5 mg/W was achieved, but pure Ag metallization appears to be competitive on this level. In a second cell batch Ag on the FS was combined with pure Cu paste on RS achieving similar η compared to the reference with only Ag metallization for 80 to 100 μm-wide contacts on the RS. The Cu group fall below the m_{Ag} mid-term target of 5 mg/W. An effect on R_{LINE} due to oxidation of the Cu fingers was not found after 24-day air exposure. But cell reliability must be addressed on module level in lifetime testing. This is planned. In a third cell batch high and low Ag consumption SHJ cells were integrated into modules. Compared to the reference layouts the η-level was maintained while the bifaciality was improved by 1 $\%_{rel.}$ and the Ag consumption was cut almost by two third (63 %).

For future work, we plan to investigate if the next generation of AgCu and Ag pastes can meet the targets of 5 and 2 mg/W with an as low as possible η-drop. Especially for 2 mg/W the focus shifts more to pure Cu pastes on the RS. The different approaches for reducing Ag consumption will be tested on cell and module level including reliability testing. For this low Ag consumption on cell level the contribution for low temperature interconnection becomes much more relevant and m_{Ag} needs to be reduced on module side as well for a more sustainable TW market [34]. This topic is addressed within Fraunhofer ISE as well.

CRediT authorship contribution statement

S. Pingel: Writing – review & editing, Writing – original draft, Visualization, Software, Methodology, Formal analysis, Conceptualization. **F.M. Maarouf:** Resources, Investigation, Conceptualization. **N. Wengenmeyr:** Resources, Investigation. **M. Linse:** Resources, Investigation. **L. Folcarelli:** Investigation. **J. Schube:** Writing – review & editing, Investigation. **S. Hoffmann:** Investigation, Conceptualization. **S. Tepner:** Writing – review & editing. **J. Huyeng:** Writing – review & editing, Supervision, Software, Funding acquisition, Conceptualization. **A. Lorenz:** Writing – review & editing, Supervision, Project administration, Funding acquisition, Conceptualization. **F. Clement:** Supervision, Project administration, Funding acquisition.

Declaration of competing interest

The authors declare the following financial interests/personal relationships which may be considered as potential competing interests: Sebastian Pingel reports equipment, drugs, or supplies was provided by Paste Suppliers. If there are other authors, they declare that they have no known competing financial interests or personal relationships that could have appeared to influence the work reported in this paper.

Acknowledgements

The authors would like to thank the co-workers at Fraunhofer ISE for their support in processing and characterization, the paste suppliers for providing test material and the Federal Ministry of Economic Affairs and Climate Action for funding the research project “Utility4Indium” under contract no. 03EE1127D and “HIT“ under contract no. 03EE1197B”.

Data availability

Data will be made available on request.

References

[1] Jonas Bartsch, The role of silver in terawatt PV production - perspectives and options, Photovoltaics Int. 48 (2022).
[2] E. Gervais, S. Herceg, S. Nold, K.-A. Weiß, Sustainability strategies for PV: framework, status and needs, EPJ Photovolt. 12 (2021) 5, https://doi.org/10.1051/epjpv/2021005.
[3] Y. Zhang, M. Kim, L. Wang, P. Verlinden, B. Hallam, Design considerations for multi-terawatt scale manufacturing of existing and future photovoltaic technologies: challenges and opportunities related to silver, indium and bismuth consumption, Energy Environ. Sci. 14 (11) (2021) 5587–5610, https://doi.org/10.1039/D1EE01814K.
[4] P.J. Verlinden, Future challenges for photovoltaic manufacturing at the terawatt level, J. Renew. Sustain. Energy 12 (5) (2020), https://doi.org/10.1063/5.0020380.
[5] Y.-C. Chang, et al., Silver-lean metallization and hybrid contacts via plating on screen-printed metal for silicon solar cells manufacturing, Prog. Photovoltaics Res. Appl. (2024), https://doi.org/10.1002/pip.3799.
[6] D. Erath, et al., Fast screen printing and curing process for silicon heterojunction solar cells, in: PROCEEDINGS OF THE 9TH WORKSHOP ON METALLIZATION AND INTERCONNECTION FOR CRYSTALLINE SILICON SOLAR CELLS, Genk, Belgium, 2021 20006.
[7] S. Pingel, et al., Progress on the reduction of silver consumption in metallization of silicon heterojunction solar cells, Sol. Energy Mater. Sol. Cells 265 (2024) 112620, https://doi.org/10.1016/j.solmat.2023.112620.
[8] K. Nakamura, K. Muramatsu, A. Tanaka, Y. Ohshita, Newly Developed Ag Coated Cu Paste for Si Hetero-Junction Solar Cell, 2018, https://doi.org/10.4229/35thEUPVSEC20182018-2AV.3.37.
[9] N. Chen, et al., Thermal stable high-efficiency copper screen printed back contact solar cells, Sol. RRL 7 (2) (2023), https://doi.org/10.1002/solr.202200874.
[10] R. Kopecek et al., "Interdigitated Back Contact Technology as Final Evolution for Industrial Crystalline Single-Junction Silicon Solar Cell,".
[11] D. Rudolph, et al., Screen printable, non-fire-through copper paste applied as busbar metallization for back contact solar cells, in: PROCEEDINGS OF THE 10TH WORKSHOP ON METALLIZATION AND INTERCONNECTION FOR CRYSTALLINE SILICON SOLAR CELLS, Genk, Belgium, 2022 20006.
[12] D. Rudolph, et al., Improvement of solder interconnections applied on back contact solar cells with low-temperature copper paste busbars, Sol. Energy Mater. Sol. Cells 264 (2024) 112603, https://doi.org/10.1016/j.solmat.2023.112603.
[13] S. Tepner, A. Lorenz, Printing technologies for silicon solar cell metallization: a comprehensive review, Prog Photovolt Res Appl., to be published (2023), https://doi.org/10.1002/pip.3674.
[14] VDMA, ITRPV - International Technology Roadmap for Photovoltaic, vol. 14, 2024. Edition.
[15] CPIA, China's Photovoltaic Industry Development Roadmap, 2023-24.
[16] A. Lorenz, et al., Rotary screen printed metallization of heterojunction solar cells: toward high-throughput production with very low silver laydown, Energy Technol. 10 (8) (2022) 2200377, https://doi.org/10.1002/ente.202200377.
[17] J. Schube, et al., FlexTrail printing as direct metallization with low silver consumption for silicon heterojunction solar cells: evaluation of solar cell and module performance, Energy Technol. 10 (12) (2022) 2200702, https://doi.org/10.1002/ente.202200702.
[18] M. Pospischil, et al., Applications of parallel dispensing in PV metallization, in: M. J.K. Bashir, T.K. Tat, H. Nisar, Y. Munusamy, W.C. Chong (Eds.), *AIP Conference Proceedings*, Volume Number 2157, *International Symposium On Green and Sustainable Technology: Conference Date, 23-26 April 2019 : Location, Perak, Malaysia*, AIP Publishing, Melville, N.Y.], 2019 20005.
[19] K. Gensowski, et al., Filament stretching during parallel dispensing – a way to reduce silver consumption in SHJ metallization, Sol. Energy Mater. Sol. Cells 245 (2022) 111871, https://doi.org/10.1016/j.solmat.2022.111871.
[20] K. Gensowski, et al., Dispensing of low-temperature silver pastes, in: 9th Workshop on Metallization and Interconnection for Crystalline Silicon Solar Cells, Virtual Event, 2020 20007.
[21] A. Lachowicz et al., "Project Ameliz: Patterning Techniques for Copper Electroplated Metallization on Heterojunction Solar Cells,".
[22] S.N. Abolmasov, A.S. Abramov, V.N. Verbitskii, G.G. Shelopin, A.V. Kochergin, E. I. Terukov, Formation of a copper contact grid on the surface of silicon heterojunction solar cells, Semiconductors 57 (10) (2023) 431–439, https://doi.org/10.1134/S1063782623090014.
[23] T. Hatt, S. Kluska, M. Yamin, J. Bartsch, M. Glatthaar, Native oxide barrier layer for selective electroplated metallization of silicon heterojunction solar cells, Sol. RRL 3 (6) (2019), https://doi.org/10.1002/solr.201900006.
[24] G. Limodio, et al., Copper-plating metallization with alternative seed layers for c-Si solar cells embedding carrier-selective passivating contacts, IEEE J. Photovoltaics 10 (2) (2020) 372–382, https://doi.org/10.1109/JPHOTOV.2019.2957671.
[25] T. Hatt, et al., Copper Electroplating for SHJ Solar Cells – Adequate Contact by Electrolyte Tuning, 2021.
[26] T. Tang et al., "Achievement of 25.54% Power Conversion Efficiency by Optimization of Current Losses at the Front Side of Silicon Heterojunction Solar Cells,".
[27] J. Yu, et al., Process challenges of high-performance silicon heterojunction solar cells with copper electrodes, Sol. Energy Mater. Sol. Cells 250 (2023) 112057, https://doi.org/10.1016/j.solmat.2022.112057.
[28] A. Kraft, C. Wolf, J. Bartsch, M. Glatthaar, Characterization of copper diffusion in silicon solar cells, Energy Proc. 67 (2015) 93–100, https://doi.org/10.1016/j.egypro.2015.03.292.

[29] F. Clement, et al., Project "FINALE" - screen and printing process development for ultra-fine-line contacts below 20µm finger width, in: 36th European Photovoltaic Solar Energy Conference and Exhibition, Marseille, France, 2019, pp. 255–258.
[30] T. Wenzel, et al., Progress with screen printed metallization of silicon solar cells - towards 20 µm line width and 20 mg silver laydown for PERC front side contacts, Sol. Energy Mater. Sol. Cells 244 (2022) 111804, https://doi.org/10.1016/j.solmat.2022.111804.
[31] T. Fellmeth, F. Clement, D. Biro, Analytical modeling of industrial-related silicon solar cells, IEEE J. Photovoltaics 4 (1) (2014) 504–513, https://doi.org/10.1109/JPHOTOV.2013.2281105.
[32] Ocean Tang, Progress in Development of Fusion HJT Paste: 14.12.2023, Taiyang News, 2023 [Online], https://www.youtube.com/watch?v=B27n0L2-KV4. (Accessed 24 January 2025).
[33] M. Rauer, et al., Assessing current-voltage measurements of busbarless solar cells, Sol. Energy Mater. Sol. Cells 248 (2022) 111988, https://doi.org/10.1016/j.solmat.2022.111988.
[34] D. Güldali, A. de Rose, M. Mittag, B. Grübel, U.T.H. Neuhaus, Interconnection of low-temperature metallization on silicon solar cells - the role of silver in tin-bismuth-based solder alloys, Sol. Energy Mater. Sol. Cells 285 (2025) 113488, https://doi.org/10.1016/j.solmat.2025.113488.